Power-Based Control of Low-Voltage Microgrids

Article *in* IEEE Journal of Emerging and Selected Topics in Power Electronics · December 2015

DOI: 10.1109/JESTPE.2015.2413361

CITATIONS
48

READS
279

4 authors, including:

Tommaso Caldognetto
University of Padova
74 PUBLICATIONS **767** CITATIONS
SEE PROFILE

P. Tenti
University of Padova
158 PUBLICATIONS **4,507** CITATIONS
SEE PROFILE

Danilo Iglesias Brandao
Federal University of Minas Gerais
122 PUBLICATIONS **732** CITATIONS
SEE PROFILE

This article has been accepted for publication in a future issue of this journal, but has not been fully edited. Content may change prior to final publication. Citation information: DOI 10.1109/JESTPE.2015.2413361, IEEE Journal of Emerging and Selected Topics in Power Electronics

Power-Based Control of Low-Voltage Microgrids

Tommaso Caldognetto, *Student Member, IEEE,* Simone Buso, *Member, IEEE,* Paolo Tenti, *Fellow, IEEE,* Danilo Iglesias Brandao, *Student Member, IEEE*

***Abstract*—This paper presents a simple and robust control technique for distributed energy resources in microgrids. The technique utilizes the full potential of distributed energy resources, during grid-connected and islanded operating modes. In grid-connected mode, the control pursues quasi-optimum operation of the microgrid, so as to reduce distribution losses and voltage deviations, while fully exploiting renewable energy sources. In islanded mode, it manages effectively any available energy source, including storage devices, to ensure a safe and smooth autonomous operation of the microgrid. Besides, prompt adaptation to variations of the generated and absorbed power is ensured in each operating condition. The proposed control can be implemented by an ICT architecture which is inherently flexible and scalable, allows plug-and-play integration of distributed energy sources, and does not involve time-critical communications.**

***Index Terms*—Distributed Energy Resources; Energy gateways; Low-voltage microgrids; Master-slave control; Power sharing.**

I. Introduction

THE INCREASING penetration of distributed energy resources (DERs) interfaced with the distribution grid by means of electronic power processors poses new control requirements and, at the same time, enables new efficient operating regimes for low-voltage microgrids [1], [2]. The challenge lies in the necessity of allowing prompt and effective integration of distributed and heterogeneous energy resources which, in turn, calls for flexible and scalable supporting infrastructures and plug-and-play connection standards [3], [4]. These requirements, in conjunction with the need to prevent detrimental interaction of distributed control agents, make the control problem a crucial issue for the actual development of low-voltage microgrids. Important contributions to the study of the architecture and management of microgrids are brought by research on droop-based networks [4]–[6] and on the optimal control techniques for these complex systems, whose typical goals are, e.g., the minimization of distribution losses [7]–[9], the definition of communication structures [10], and the effective management of transient conditions [11].

This work presents a simple, flexible, and scalable control approach where DERs behave as current sources, according to the requirements of most international grid connection standards (e.g., [12], [13]), and are dynamically managed by a master controller on the basis of the instantaneous generated and consumed power within the microgrid. The master controller resides in the Utility Interface (UI), which is an electronic power processor equipped with energy storage, connected at the point of common coupling (PCC) with the utility. In grid-connected mode, the UI performs as a voltage source synchronized with the mains, while in islanded mode it becomes the voltage-forming device for the whole microgrid.

The UI communicates with distributed units via narrowband communication links and drives them by means of active and reactive power commands [14]. This minimizes the amount of data exchange and allows the control to dynamically adapt to the actual number and capability of DERs. Moreover, new DERs can plug-and-play connect to the grid by simply sending a connection request to the master controller.

Due to its simple implementation and good performance, the proposed control approach represents a viable alternative to other solutions described in literature. It features excellent stability, good robustness to grid parameter variations, avoidance of saturation of the power capability of generation units, and fast dynamic response. From this standpoint, it shows competitive performance as compared to the most advanced droop-based control approaches [6], [15], [16], and it is less demanding in terms of network knowledge as compared to optimum control approaches [17]–[19].

II. System Architecture

Fig. 1 shows the general microgrid structure considered in this paper. It features N active nodes, M passive nodes, and a Utility Interface. Each active node hosts an energy resource, i.e., a distributed generator (DG) or an energy storage unit (ES) or both, whose power flow to the grid is controlled by an energy gateway (EG). The latter is an electronic power processor equipped with local control and communication units; its ideal structure and control functionalities are reported, e.g., in [20] and in [21]. As mentioned before, EGs are always controlled as current sources. The passive nodes include loads only, and are not necessarily endowed with smart meters.

The UI is a three-phase grid-interactive inverter equipped with energy storage (e.g., battery or super-cap) and, if necessary, with a backup generator (e.g., micro-turbine, fuel cell, diesel gen-set). It permanently performs as a voltage source, and behaves as grid-supporting unit in grid-connected operation and as grid-forming unit in islanded operation [22].

An ICT infrastructure provides the communication link (either wired or wireless) between the UI at the PCC and the EGs spread over the grid, enabling a synergistic operation of active nodes.

The proposed microgrid architecture implements all functionalities of primary, secondary, and tertiary control. In particular:

Manuscript received November 20, 2014; revised January 11, and March 2, 2015; accepted 5 March, 2015; date of current version March 07, 2015.

T. Caldognetto, S. Buso, and P. Tenti are with the Department of Information Engineering, University of Padova, 35131 Padova, Italy (e-mail: [name].[surname]@dei.unipd.it)

D. I. Brandao is with the Department of Systems and Energy, University of Campinas, 13083852 Campinas, Brazil (e-mail:dbrandao@dsce.fee.unicamp.br)

This article has been accepted for publication in a future issue of this journal, but has not been fully edited. Content may change prior to final publication. Citation information: DOI 10.1109/JESTPE.2015.2413361, IEEE Journal of Emerging and Selected Topics in Power Electronics

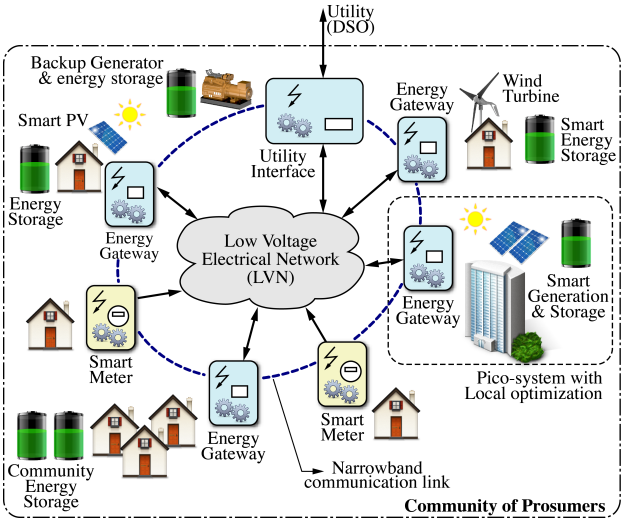

Fig. 1. General microgrid structure.

- Primary control aims at effective management of local energy resources, both generating and storage units. It guarantees local voltage support, reactive and harmonic compensation of local loads, fast reaction to power steps and voltage ride-through capability. EGs are required to implement it.
- Secondary control aims at the safe and efficient management of the entire microgrid. To this purpose, the load power demand must be shared among DERs in a way which prevents saturation of their power capability while minimizing power losses. Secondary control is also in charge of safely managing the microgrid during the transitions from grid-connected to islanded operation and *vice-versa*, and this requires synergistic operation of UI and EGs. It will be shown that these features can be achieved by a master-slave control architecture where distributed units are driven by time-averaged active and reactive power commands (power-based control).
- Tertiary control aims at achieving good power factor and flexible interaction between utility and microgrid by ensuring demand response capability, day-ahead planning and high power factor at the PCC. The former requirements are met by the synergistic operation of active units (UI and EGs), that is based on short-term and long-term planning of energy storage and of backup power units. Instead, high power factor at PCC is ensured by the inner control loops of the UI, that perform real-time compensation of the residual unbalance, reactive, and harmonic currents drawn by the loads.

Note finally that, with the proposed architecture, the UI is the only voltage-forming unit during islanded operation. Accordingly, it acts as voltage and frequency reference for the entire microgrid. Suitable hardware redundancy is required to ensure continuity in case of fault.

In the following, we describe a power-based master-slave control technique where a master controller (MC) drives all distributed units (UI and EGs) to pursue the goals of secondary and tertiary control. To this purpose, each active unit contributes to the microgrid power needs in proportion of its power capability. This leads to a uniform utilization of DERs and equalizes the thermal stress in the EGs. It will also be shown that the inner control loops of the Utility Interface ensure fast reaction to load steps, good power factor at PCC and safe transition to islanded operation.

III. Data Collection and Processing

At the beginning of each control cycle, which equals a few periods of line voltage, the MC polls each active node of the microgrid. The EGs return the amount of their power capability that can be shared with the microgrid, taking into account the locally generated power and the stored energy.

Then the MC computes the power contribution required to each active node in the next cycle based on the data collected by responding EGs and the power flow measured at PCC.

Periodically, the MC also broadcasts a *call for active agents*, and all the EGs which are currently active in the microgrid identify themselves and are added to the list of active agents. This allows, on the one hand, a periodic update of the microgrid agents and, on the other hand, easy and fast plug-and-play connection (or disconnection) of DERs.

A. Data Collection

More in detail, the centralized control strategy performs as follows. At the end of the ℓ-th control cycle, the MC determines the total active power $P_{PCC}(\ell)$ and reactive power $Q_{PCC}(\ell)$ absorbed by the microgrid at PCC during that cycle. This power is equal to the sum of the power drawn from the mains (i.e., P_{GRID}, Q_{GRID}) and the power delivered by the UI (i.e., P_{UI}, Q_{UI}). Moreover, the *local controller* of the n-th EG ($n = 1, \ldots, N$) sends the following data to the MC:

- the active power $P_{Gn}(\ell)$ and the reactive power $Q_{Gn}(\ell)$ generated during the ℓ-th control cycle;
- the estimated active power $\hat{P}_{Gn}(\ell+1)$ that will be generated locally in the next control cycle;
- the estimated minimum active power $\hat{P}_{Gn}^{\min}(\ell+1)$ and maximum active power $\hat{P}_{Gn}^{\max}(\ell+1)$ that the node can generate in the following cycle by taking advantage of the maximum power that can be delivered ($\hat{P}_{Sn}^{\text{out}}$) or absorbed ($\hat{P}_{Sn}^{\text{in}}$) by the local energy storage unit, if any. We have:

$$\begin{cases} \hat{P}_{Gn}^{\min}(\ell+1) = \hat{P}_{Gn}(\ell+1) - \hat{P}_{Sn}^{\text{in}}(\ell+1) \\ \hat{P}_{Gn}^{\max}(\ell+1) = \hat{P}_{Gn}(\ell+1) + \hat{P}_{Sn}^{\text{out}}(\ell+1) \end{cases}, \quad (1)$$

during grid-connected operation, and

$$\begin{cases} \hat{P}_{Gn}^{\min}(\ell+1) = -\hat{P}_{Sn}^{\text{in}}(\ell+1) \\ \hat{P}_{Gn}^{\max}(\ell+1) = \hat{P}_{Gn}(\ell+1) + \hat{P}_{Sn}^{\text{out}}(\ell+1) \end{cases}, \quad (2)$$

during islanded operation;

- the rated apparent power $\hat{A}_{Gn}(\ell+1)$ of the EG inverter and its temporary overloading capability $\hat{A}_{Gn}^{\text{over}}(\ell+1)$.

In a basic implementation, the estimated quantities for cycle $\ell+1$ are simply considered equal to the values at control cycle ℓ. In more advanced implementations, during grid-connected operation it is possible to take advantage of additional information (e.g., node voltage statistics, weather forecasts) to

This article has been accepted for publication in a future issue of this journal, but has not been fully edited. Content may change prior to final publication. Citation information: DOI 10.1109/JESTPE.2015.2413361, IEEE Journal of Emerging and Selected Topics in Power Electronics

learn how to conveniently define, on a long-term basis, the parameters $\hat{P}_{Sn}^{\text{out}}$ and $\hat{P}_{Sn}^{\text{in}}$, for example, in order to maximize the local energy production.

We observe how definitions (1) and (2) given for the estimated minimum active power $\hat{P}_{Gn}^{\min}$ reflect the different control priorities in grid-connected and islanded operation. Indeed, during grid-connected operation it is more advantageous to extract all the power available from renewables, e.g., by operating PV sources at their maximum power point, whereas during islanded operation it is of paramount importance to guarantee the active power balance for the islanded system. In this light, $\hat{P}_{Gn}^{\min}$ is set equal to $\hat{P}_{Gn} - \hat{P}_{Sn}^{\text{in}}$ during grid-connected mode, so that each EG would at least inject the power produced from the local source, independently from the state of charge of the local energy storage, and equal to $-\hat{P}_{Sn}^{\text{in}}$, during islanded mode, to allow the EGs to provide non-positive active power injection when generation exceeds absorption.

B. Processing

Based on the collected data, the *master controller* determines:

- the total active and reactive power delivered by DERs along cycle ℓ:

$$P_{Gtot}(\ell) = \sum_{n=1}^{N} P_{Gn}(\ell) \,, \tag{3}$$

$$Q_{Gtot}(\ell) = \sum_{n=1}^{N} Q_{Gn}(\ell) \,; \tag{4}$$

- the total active and reactive power absorbed within the microgrid along cycle ℓ:

$$P_{Ltot}(\ell) = P_{PCC}(\ell) + P_{Gtot}(\ell) \,, \tag{5}$$

$$Q_{Ltot}(\ell) = Q_{PCC}(\ell) + Q_{Gtot}(\ell) \,; \tag{6}$$

- the estimated active power $\hat{P}_{Ltot}(\ell+1)$ and reactive power $\hat{Q}_{Ltot}(\ell+1)$ that will be absorbed by microgrid loads in the next control cycle $\ell+1$ and the reference for the total power $P_{Gtot}^{*}(\ell+1)$, $Q_{Gtot}^{*}(\ell+1)$ to be delivered by EGs:

$$\begin{aligned} \hat{P}_{Ltot}(\ell+1) &= P_{Ltot}(\ell) \\ P_{Gtot}^{*}(\ell+1) &= \hat{P}_{Ltot}(\ell+1) - P_{PCC}^{*}(\ell+1) \end{aligned} \,, \tag{7}$$

$$\begin{aligned} \hat{Q}_{Ltot}(\ell+1) &= Q_{Ltot}(\ell) \\ Q_{Gtot}^{*}(\ell+1) &= \hat{Q}_{Ltot}(\ell+1) - Q_{PCC}^{*}(\ell+1) \end{aligned} \,, \tag{8}$$

  where $P_{PCC}^{*}(\ell+1)$ and $Q_{PCC}^{*}(\ell+1)$ represent the assigned reference power flow at the PCC for the next control cycle;
- the estimated total active power generated by DERs in cycle $\ell+1$ and the corresponding upper and lower limits:

$$\hat{P}_{Gtot}(\ell+1) = \sum_{n=1}^{N} \hat{P}_{Gn}(\ell+1) \,, \tag{9}$$

$$\hat{P}_{Gtot}^{\min}(\ell+1) = \sum_{n=1}^{N} \hat{P}_{Gn}^{\min}(\ell+1) \,, \tag{10}$$

$$\hat{P}_{Gtot}^{\max}(\ell+1) = \sum_{n=1}^{N} \hat{P}_{Gn}^{\max}(\ell+1) \,; \tag{11}$$

- the estimated maximum reactive power that the active nodes can deliver in normal operation or in overloading condition in cycle $\ell+1$:

$$\begin{aligned} \hat{Q}_{Gn}^{\max}(\ell+1) &= \sqrt{\hat{A}_{Gn}^{2}(\ell+1) - \hat{P}_{Gn}^{2}(\ell+1)} \\ \hat{Q}_{Gtot}^{\max}(\ell+1) &= \sum_{n=1}^{N} \hat{Q}_{Gn}^{\max}(\ell+1) \end{aligned} \,, \tag{12}$$

$$\begin{aligned} \hat{Q}_{Gn}^{\text{over}}(\ell+1) &= \sqrt{\hat{A}_{Gn}^{\text{over}\,2}(\ell+1) - \hat{P}_{Gn}^{2}(\ell+1)} \\ \hat{Q}_{Gtot}^{\text{over}}(\ell+1) &= \sum_{n=1}^{N} \hat{Q}_{Gn}^{\text{over}}(\ell+1) \end{aligned} \,. \tag{13}$$

Based on the global status of controllable DERs (i.e., EGs) obtained above, the MC regulates the power flow at the PCC to track the references P_{PCC}^{*}, Q_{PCC}^{*}, given a fixed power flow from the main grid P_{GRID}^{*}, Q_{GRID}^{*}. Accordingly, the power exchange at the terminals of the UI are:

$$\hat{P}_{UI}(\ell+1) = P_{PCC}^{*}(\ell+1) - P_{GRID}^{*}(\ell+1) \,, \tag{14}$$

$$\hat{Q}_{UI}(\ell+1) = Q_{PCC}^{*}(\ell+1) - Q_{GRID}^{*}(\ell+1) \,. \tag{15}$$

While references P_{GRID}^{*}, Q_{GRID}^{*}, that are actuated by the UI [22], [23], are either set according to the negotiation on energy exchange with the DSO (taking place in the tertiary control layer [5]) or set to zero during the islanded operating mode, references P_{PCC}^{*}, Q_{PCC}^{*} are set by the MC according to the energy state of the UI, like, e.g., in [24].

IV. Power-Based Control

The estimated quantities (7)-(13) are the input data for the control algorithm that drives the distributed EGs. In order to actuate it, the MC generates two control variables α_P and α_Q (both ranging in the interval $[0, 2]$), which are then *broadcasted* to all the EGs, i.e., *applied to the whole microgrid*. We first describe the control algorithm for islanded operation, which is then easily adapted to grid-connected mode.

A. Active Power Control

The active power is controlled by variable α_P, which is set by the MC depending on the operation mode. We distinguish four operating modes:

1) $P_{Gtot}^{*}(\ell+1) < \hat{P}_{Gtot}^{\min}(\ell+1)$*:* in this case, the loads are expected to absorb a total active power lower than the minimum power the active nodes can deliver. As a result, the MC sets:

$$\alpha_P = 0 \,, \tag{16}$$

and each EG sets its active power reference $P_{Gn}^{*}(\ell+1)$ at the minimum allowed value:

$$P_{Gn}^{*}(\ell+1) = \hat{P}_{Gn}^{\min}(\ell+1) \,. \tag{17}$$

This article has been accepted for publication in a future issue of this journal, but has not been fully edited. Content may change prior to final publication. Citation information: DOI 10.1109/JESTPE.2015.2413361, IEEE Journal of Emerging and Selected Topics in Power Electronics

The power balance can temporarily be ensured by diverting the power in excess to the UI, that stores it in its energy storage device, as described in [25]. Of course, this situation can be sustained for a limited time, then loads and/or generators must be readjusted (e.g., MPPT's must be de-tuned so as to extract less power) to restore the equilibrium.

2) $\hat{P}^{\min}_{Gtot}(\ell+1) \leq P^{*}_{Gtot}(\ell+1) < \hat{P}_{Gtot}(\ell+1)$*:* the expected load power is lower than the generated power but the excess of generation can be temporarily diverted into distributed storage units. In this case, the UI does not contribute to power balance, and the MC sets the value of α_P as:

$$\alpha_P = \frac{P^{*}_{Gtot}(\ell+1) - \hat{P}^{\min}_{Gtot}(\ell+1)}{\hat{P}_{Gtot}(\ell+1) - \hat{P}^{\min}_{Gtot}(\ell+1)},\ 0 \leq \alpha_P \leq 1\,. \quad (18)$$

Correspondingly, each active node sets its active power reference as:

$$\begin{aligned} P^{*}_{Gn}(\ell+1) &= \hat{P}^{\min}_{Gn}(\ell+1) + \\ &+\alpha_P \left(\hat{P}_{Gn}(\ell+1) - \hat{P}^{\min}_{Gn}(\ell+1)\right). \end{aligned} \quad (19)$$

3) $\hat{P}_{Gtot}(\ell+1) \leq P^{*}_{Gtot}(\ell+1) \leq \hat{P}^{\max}_{Gtot}(\ell+1)$*:* the expected load power is higher than generated power but the difference can be supported, temporarily, by distributed energy storage. In this case, the UI does not contribute to power balance, and the MC sets the value of α_P as:

$$\alpha_P = 1 + \frac{P^{*}_{Gtot}(\ell+1) - \hat{P}_{Gtot}(\ell+1)}{\hat{P}^{\max}_{Gtot}(\ell+1) - \hat{P}_{Gtot}(\ell+1)},\ 1 \leq \alpha_P \leq 2. \quad (20)$$

Correspondingly, each active node sets its active power reference as:

$$\begin{aligned} P^{*}_{Gn}(\ell+1) &= \hat{P}_{Gn}(\ell+1) + \\ &+(\alpha_P - 1)\left(\hat{P}^{\max}_{Gn}(\ell+1) - \hat{P}_{Gn}(\ell+1)\right). \end{aligned} \quad (21)$$

4) $P^{*}_{Gtot}(\ell+1) > \hat{P}^{\max}_{Gtot}(\ell+1)$*:* the loads are expected to absorb a total power which is greater than the maximum power the active nodes can deliver. In this case the MC sets:

$$\alpha_P = 2\,. \quad (22)$$

Correspondingly, each active node sets its active power reference as:

$$P^{*}_{Gn}(\ell+1) = \hat{P}^{\max}_{Gn}(\ell+1)\,. \quad (23)$$

The power balance can temporarily be ensured at the expense of the energy stored in the UI. After some time, of course, some of the loads and/or generators will have to be readjusted to restore the equilibrium.

B. Reactive Power Control

The reactive power is controlled by variable α_Q, which is set by the MC depending on the operation mode. There are two operation modes:

1) $Q^{*}_{Gtot}(\ell+1) \leq \hat{Q}^{\max}_{Gtot}(\ell+1)$*:* load requirements can be met by distributed EGs. In this case the MC sets:

$$\alpha_Q = \frac{Q^{*}_{Gtot}(\ell+1)}{\hat{Q}^{\max}_{Gtot}(\ell+1)},\ 0 \leq \alpha_Q \leq 1\,. \quad (24)$$

Correspondingly, each active node sets its reactive power reference as:

$$Q^{*}_{Gn}(\ell+1) = \alpha_Q \cdot \hat{Q}^{\max}_{Gn}(\ell+1)\,. \quad (25)$$

2) $Q^{*}_{Gtot}(\ell+1) > \hat{Q}^{\max}_{Gtot}(\ell+1)$*:* loads requirement can only be met by overloading the EGs. In this case the MC sets:

$$\alpha_Q = 1 + \frac{Q^{*}_{Gtot}(\ell+1) - \hat{Q}^{\max}_{Gtot}(\ell+1)}{\hat{Q}^{\text{over}}_{Gtot}(\ell+1) - \hat{Q}^{\max}_{Gtot}(\ell+1)},\ 1 < \alpha_Q \leq 2\,. \quad (26)$$

Correspondingly, each active node sets its reactive power reference as:

$$\begin{aligned} Q^{*}_{Gn}(\ell+1) &= \hat{Q}^{\max}_{Gn}(\ell+1) + \\ &+(\alpha_Q - 1)\left(\hat{Q}^{\text{over}}_{Gn}(\ell+1) - \hat{Q}^{\max}_{Gn}(\ell+1)\right). \end{aligned} \quad (27)$$

A simplified block diagram representing the main operations of the power based control for what concerns active power balance is shown in Fig. 2; a corresponding scheme can be derived for reactive power control. Gain errors and off-set errors are included to take into account the main non idealities of a realistic application case. In general, gain errors affect the loop gain of the feedback system and have to be considered to assess system stability, whereas off-set errors have to be taken into account to analyze its steady-state accuracy in regulating the controlled quantities. In Fig. 2(a), variables γ^{g}_{Gn} and P^{err}_{Gn} represent the gain and off-set errors made by EGs in producing the assigned power reference P^{*}_{Gn}; γ^{m}_{Gn} and γ^{m}_{PCC} represent the gain errors of measurement instruments, while off-set errors in measurements are, for now, neglected. On the base of Fig. 2(a), the simplified model of Fig. 2(b) can be drawn, that is used for the analysis of the power based control stability.

By employing the block diagram of Fig. 2(b) we can derive the discrete time transfer function between the total absorbed power P_{Ltot} and the reference P^{*}_{Gtot}. By neglecting the reference input P^{*}_{PCC}, since it varies very slowly, as mentioned in Section III-B, it is possible to find:

$$P^{*}_{Gtot}(z) = \frac{\gamma^{m}_{PCC}}{z + \gamma^{g}_{G}\left(\gamma^{m}_{G} - \gamma^{m}_{PCC}\right)} P_{Ltot}(z)\,. \quad (28)$$

Equation (28) shows that, if the system is ideal (i.e., γ^{g}_{Gn}, γ^{m}_{Gn}, γ^{m}_{PCC} are equal to one and P^{err}_{Gn} is equal to zero) then the power reference EGs are committed to is going to track the total absorbed power in the microgrid (with one control cycle delay); secondly, that the stability condition for active power reference generation, in general, can be expressed as: $|\gamma^{g}_{G}(\gamma^{m}_{G} - \gamma^{m}_{PCC})| < 1$, that can easily be met by any commercial power meter. This proves a stable control operation for the operating modes *2)* and *3)* referred to in Section IV-A.

The diagrams in Fig. 2 also highlight that, if the power requested by the load exceeds the total power capability of EGs, the coefficient α_P seamlessly saturates to its upper limit, so that each EG continuously delivers the maximum power that is locally available ($P^{\max}_{Gn}$). When the opposite situation occurs, i.e., the minimum injectable power from EGs is higher than the load power, the coefficient α_P is automatically saturated at its lower limit and each EG continuously delivers the minimum power ($P^{\min}_{Gn}$). Because the control system operates on a cycle by cycle basis, with no memory of the grid state during previous cycles, a stable control operation is

This article has been accepted for publication in a future issue of this journal, but has not been fully edited. Content may change prior to final publication. Citation information: DOI 10.1109/JESTPE.2015.2413361, IEEE Journal of Emerging and Selected Topics in Power Electronics

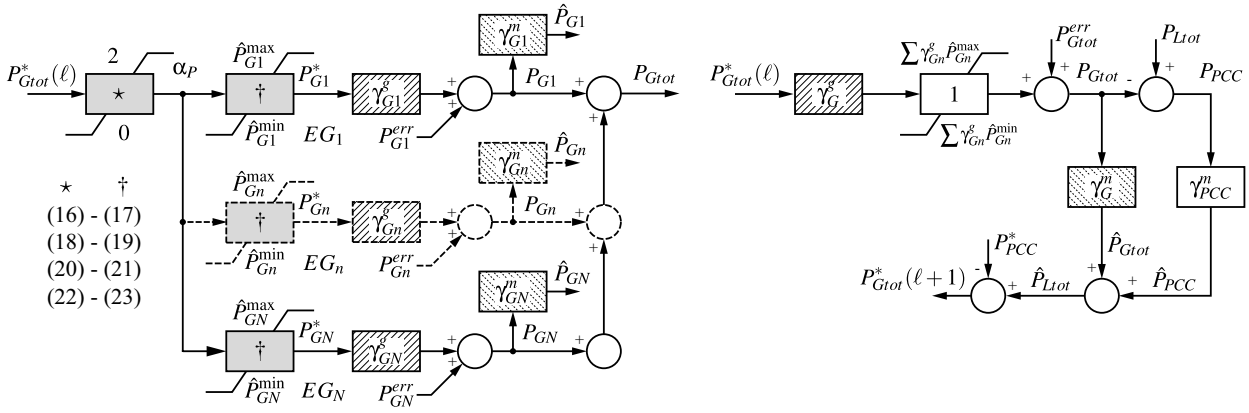

(a) Generation of power commands.

(b) Calculation of power references.

Fig. 2. Simplified model of the power-based control.

guaranteed, as well, for the operating modes *1)* and *4)* referred to in Section IV-A.

For what concerns the regulation accuracy of the power flow at the PCC, we first observe that:

$$P_{PCC}(\ell) = P_{Ltot}(\ell) - \gamma^g_G \hat{P}^*_{Gtot}(\ell) - P^{err}_{Gtot}(\ell), \qquad (29)$$

where P_{PCC} is shared among the UI (P_{UI}) and the mains (P_{GRID}) [equations (14)-(15)] according to the negotiation on energy exchange with the DSO taking place in the tertiary control layer. From (29), the power flow at the PCC is equal to the power reference P_{PCC} minus the error introduced by EGs. This error can be canceled by the MC, e.g., employing a local integrative regulator to properly modulate the power term P_{PCC} [24]. Similarly, the fluctuations in local power production can be modeled as exogenous inputs, that only affect the limits $\hat{P}^{\min}_{Gn}$ and $\hat{P}^{\max}_{Gn}$ and do not impair the stability of the system. The limits are acquired and processed by the MC at each control cycle, allowing to accordingly update the control commands to EGs, so as to account for the actual generation profile. Finally, although temporary mismatches (i.e., lasting few line cycles) among the effectively generated power and its estimate can have an effect on the injected power, this can be limited by a proper design of EG hardware. In any case, DC-link voltage deviations caused by abrupt changes in operating conditions, which may affect primarily voltage controlled inverters [6], are attenuated in the considered EG structure thanks to the adopted current controlled approach [26].

C. Grid-connected mode: active and reactive power control

While operating connected to the mains, the above control strategy can easily be adapted to obtain a conventional grid-connected operation, where DERs simply inject the locally generated power in compliance with grid standards. In fact, in this case, the MC can simply set $\alpha_P = 1$, causing the total power generated by DERs to be injected into the grid. Local power needs (e.g., to restore the state of charge of the ES at the nominal value) can be considered by correcting the estimates of generated power $\hat{P}_{Gn}(\ell+1)$. In any case, the power balance is ensured by the utility grid.

As far as reactive power compensation is concerned, the UI first decides its contribution Q_{UI} for the next control cycle. Then, it adjusts the total reactive power requested to the EGs according to the equation:

$$Q^*_{Gtot}(\ell+1) = \hat{Q}_{Ltot}(\ell) - Q_{UI}(\ell+1). \qquad (30)$$

Both for active and reactive power, the UI can also distribute the references differently in the three phases to compensate load unbalance.

V. Control Features and Node Voltage Regulation

The centralized control strategy presented above has several advantages. First of all, the execution of calculated power commands does not require any synchronization among nodes. In fact, power commands can be executed by controlling the phase shift between local voltage and current through, e.g., a phase-locked loop, without the need to synchronize to an external common time base. Sophisticated PMUs (Phase Measurement Units) are therefore not needed, and phasor control, which can be critical in low-voltage grids, can be avoided.

Second, every EG can implement the power commands by acting on the current control loop of its inverter, resulting in wide bandwidth and high dynamic output impedance.

Third, since EGs dynamically perform as current sources, they are minimizing their impact on the grid branch impedances. As a result, possible dynamic variations of such impedances are avoided, preventing potential stability issues. Besides, specific provisions can be taken at the current control layer of distributed resources to further improve grid resonance damping [27], [28].

Fourth, every active node communicates only with the master controller, that returns the control set-points in the form of broadcasted signals. The required data rate is therefore very low, which allows safe and reliable transmission protocols to be implemented, so as to increase communication robustness.

Fifth, the above control algorithm can easily be modified to include voltage regulation strategies [29]–[31] at each active node. Indeed, the controller model for the EGs adopted in

This article has been accepted for publication in a future issue of this journal, but has not been fully edited. Content may change prior to final publication. Citation information: DOI 10.1109/JESTPE.2015.2413361, IEEE Journal of Emerging and Selected Topics in Power Electronics

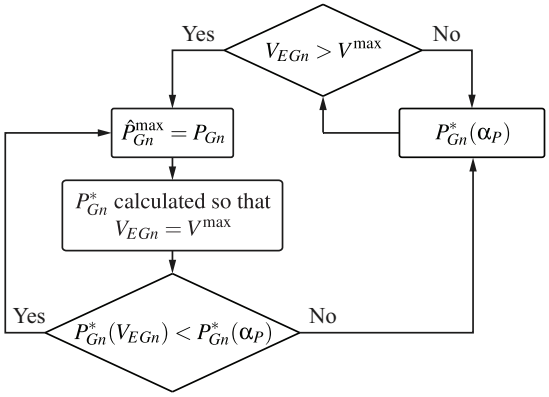

Fig. 3. Overvoltage control scheme.

the application example of Section VI, includes the automatic overvoltage limitation technique represented in Fig. 3. It ensures that the voltage amplitude at active grid nodes does not exceed the allowable upper limit $V^{\max}$. According to the scheme, if the n-th EG detects an overvoltage condition, i.e., if $V_{EGn} > V^{\max}$, then its active power reference P_{Gn}^{*} becomes regulated locally, on the basis of the measured output voltage magnitude V_{EGn}, so that $V_{EGn} = V^{\max}$. Accordingly, the resulting $P_{Gn}^{*}(V_{EGn})$ is the maximum power that the node can generate in this situation. The overvoltage condition is cleared when the power reference $P_{Gn}^{*}(\alpha_P)$, that is determined on the base of the received α_P coefficient and the actual local power availability, is lower than the locally calculated reference $P_{Gn}^{*}(V_{EGn})$.

VI. Application Example

The proposed power-based (PB) control technique has been tested for different network topologies and operating conditions, both static and dynamic, in grid-connected and islanded mode. To clearly illustrate the control features, we consider here the simple microgrid setup shown in Fig. 4. It includes two EGs, one load, and the UI.

The considered power system is low-voltage and the parameters of the adopted power electronic interfaces, photovoltaic (PV) sources, and storage units are those of commercial devices suited for residential applications. Distribution grid parameters are reported in Table I, while the parameters of EG_1 and EG_2 are shown in Table II and Table III, respectively. A narrowband communication link provides the required information exchange between the UI and the couple of EGs.

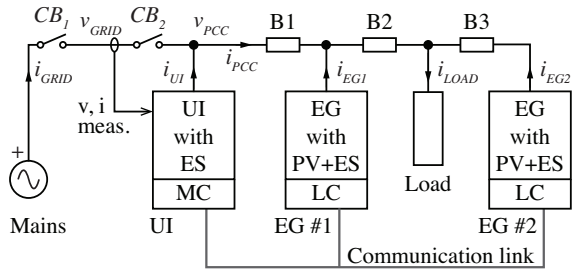

Fig. 4. Considered LV power system.

TABLE I
Distribution grid parameters

Parameter	Symbol	Value	
Grid voltage	V_{GRID}	230	V
Grid frequency	f_{GRID}	50	Hz
Max. voltage deviation	$\Delta v_{\%}^{\max}$	4.0	%
B_1 impedance	Z_{B1}	$0.17 + j0.04$	Ω
B_2 impedance	Z_{B2}	$0.26 + j0.06$	Ω
B_3 impedance	Z_{B3}	$0.70 + j0.16$	Ω
Load power factor	PF	0.95	-

TABLE II
First energy gateway parameters (EG#1)

Parameter	Symbol	Value	
EG power rating	A_{EG1}	4.2	kVA
EG overload power rating	A_{EG1}^{over}	4.6	kVA
EG nominal efficiency	η_{EG1}	0.95	-
PV nominal power rating	P_{PV1}	4.0	kW
ES capacity	E_{ES1}	3.6	kWh
ES max discharging power	$P_{S1}^{\text{out(max)}}$	2.0	kW
ES max recharging power	$P_{S1}^{\text{in(max)}}$	1.0	kW
ES charging efficiency	$\eta_{ES1,Rec}$	0.92	-
ES discharging efficiency	$\eta_{ES,Disc}$	0.92	-

TABLE III
Second energy gateway parameters (EG#2)

Parameter	Symbol	Value	
EG power rating	A_{EG2}	5.0	kVA
EG overload power rating	A_{EG2}^{over}	5.4	kVA
EG nominal efficiency	η_{EG2}	0.95	-
PV nominal power rating	P_{PV2}	4.0	kW
ES capacity	E_{ES2}	5.4	kWh
ES max discharging power	$P_{S2}^{\text{out(max)}}$	3.0	kW
ES max recharging power	$P_{S2}^{\text{in(max)}}$	1.5	kW
ES charging efficiency	$\eta_{ES2,Rec}$	0.92	-
ES discharging efficiency	$\eta_{ES,Disc}$	0.92	-

A. Simulation Results

The results obtained from the simulation of the low-voltage power system of Fig. 4 in response to typical absorption and generation profiles are discussed in the following. In order to highlight the effect of the proposed control approach on the microgrid performance, three specific cases of operation are considered:

- *Case A – No PB control:* in this case the EGs are not equipped with local energy storage and operate independently, injecting into the grid the total active power extracted from the local PV source. No communication and reactive power compensation is implemented.
- *Case B – PB control:* in this case EGs are not equipped with local energy storage and operate under the supervision of the master controller. The EGs inject into the grid the active power extracted from the local PV source and the reactive power that corresponds to the received coefficient α_Q. The local *active power* generation is automatically curtailed in case of overvoltage detection.
- *Case C – PB control with distributed ES:* in this case EGs

This article has been accepted for publication in a future issue of this journal, but has not been fully edited. Content may change prior to final publication. Citation information: DOI 10.1109/JESTPE.2015.2413361, IEEE Journal of Emerging and Selected Topics in Power Electronics

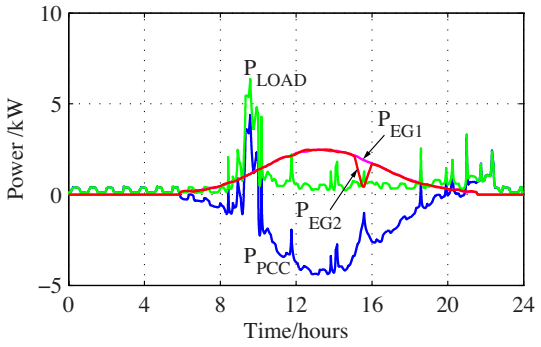

Fig. 5. Active power profiles without PB control.

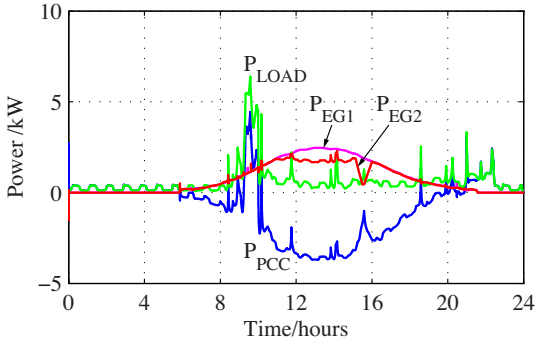

Fig. 6. Active power profiles with PB control.

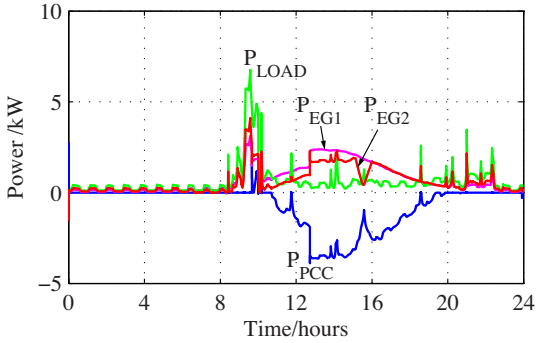

Fig. 7. Active power profiles with PB control and energy storage. Note how the peak in power demand, at 9:00 hours, is eliminated.

are equipped with local energy storage and operate under the supervision of the master controller. On the basis of the received coefficients α_P and α_Q, the EGs deliver the requested active and reactive power that correspond to the local power availability. In case of overvoltage detection, the involved EG limits its active power injection, given the mainly resistive nature of the grid branch impedances. The excess of power production is automatically curtailed or, in case of ES availability, stored locally.

1) Active power profiles: Fig. 5, Fig. 6, and Fig. 7 show the behavior of the measured active power flows for the considered cases in response to given generation and absorption profiles.

In *Case A*, Fig. 5, EG_1 and EG_2 exchange with the grid only the active power produced by the PV sources, without taking into account any overvoltage constraint at grid nodes. Then,

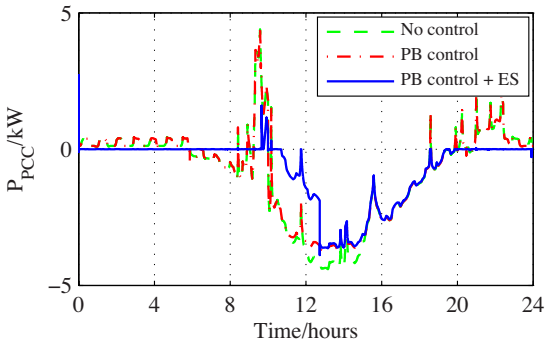

Fig. 8. Active power at PCC.

the power drawn from the PCC is equal to the total power absorbed by the load minus the total power generated by the PV sources. Consequently, the power flow at the PCC shows the same variability of generation and absorption profiles.

In *Case B*, Fig. 6, the power-based control is active. For what concerns the active power injection, when voltage magnitudes of active nodes are within nominal values, the active power flow behaviors in *Case B* and *Case A* are identical. A different situation is established for reactive power. Indeed, the power-based control instructs the EGs to completely compensate the net reactive power produced within the microgrid, thus causing a constant zero reactive power exchange at the PCC. Further details are given with the discussion of Table IV.

In *Case C*, Fig. 7, it is shown the effect of the integration of energy storage on microgrid operation. ES enables an efficient control of the active power injection from EGs. In fact, the active power injection from EGs is now driven by the needs of the loads through the supervision of the master controller. This reflects on the active power exchanged at the PCC, which appears smoother than in *Case A* and *Case B*, thanks to the inherent *peak shaving* capability of the microgrid.

Finally, considering *Case B* and *Case C* we observe the effect of the overvoltage limitation by dynamic active power control, that causes the reduction in EG_2 power generation, needed to fulfill the imposed grid voltage magnitude constraint (see Table II, parameter $\Delta v\%^{(\max)}$).

2) Power flow at PCC: Fig. 8 shows the behavior of the active power flow through the PCC for the considered cases. As noticed in the previous paragraph, the lower variance of the power flow at PCC happens when the power-based control is active and EGs are equipped with energy storage units. In Fig. 8, the fluctuations in load power absorption during intervals $[0,\ 8]$ h and $[20, 24]$ h are completely absorbed by EGs thanks to the available energy storage. Similarly, the peak of absorption occurring at 9 h is properly redistributed among EGs (see Fig. 7) and effectively reduced at the PCC.

Distributed ES also contributes to partially absorb the overproduction from PV sources, in the interval $[10, 13]$ h, until the completion of recharge cycle.

3) Distribution losses: Fig. 9 shows the obtained distribution power losses for the considered cases. The proposed power-based control formulation inherently compensates unwanted reactive power flows within the grid in a distributed fashion. This is known to be beneficial in terms of distribution

This article has been accepted for publication in a future issue of this journal, but has not been fully edited. Content may change prior to final publication. Citation information: DOI 10.1109/JESTPE.2015.2413361, IEEE Journal of Emerging and Selected Topics in Power Electronics

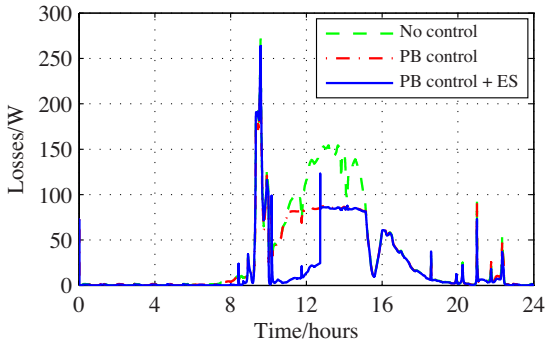

Fig. 9. Distribution power losses over the grid.

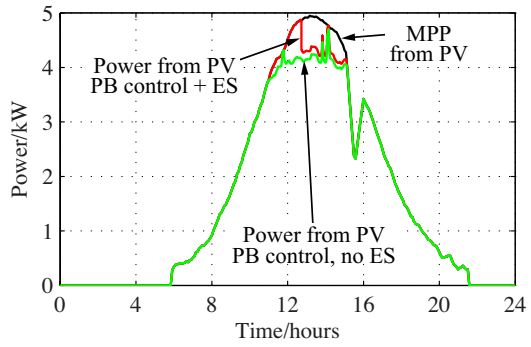

Fig. 11. Total power production from PV sources.

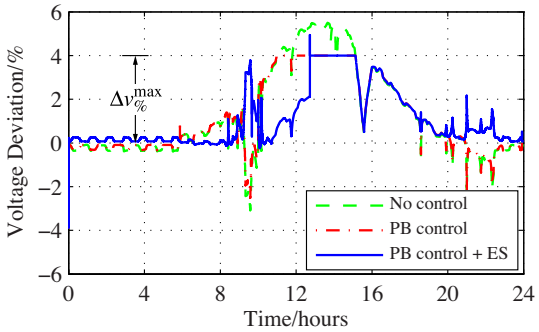

Fig. 10. Voltage deviation at EG_2 node.

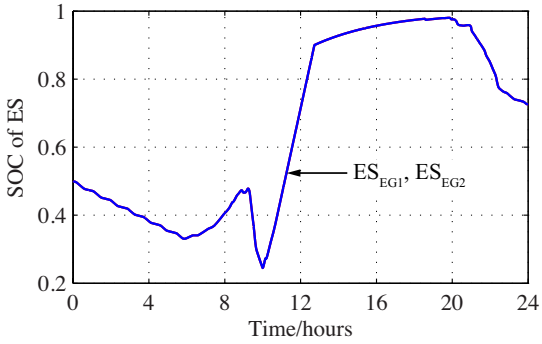

Fig. 12. State of charge of energy storage devices (*Case C*).

losses [32], [33]. Besides, the distributed energy storage, relevant for *Case C*, enables the active power control, and thus further improves the loss count by reducing circulating currents. The resulting effect on distribution losses can be noticed in interval $[10, 12]$ h of Fig. 9, where distribution losses in *Case C* are significantly lower than those measured in *Case A* and *Case B*.

4) Voltage deviations at grid nodes: Low-voltage distribution lines are mainly resistive [4], therefore, the active power flow significantly affects voltage amplitudes at grid nodes. Indeed, during periods of peak production from renewables, undesirable voltage deviations from nominal values can be registered due to abnormal active power injection. In the considered simulation setup, overvoltage conditions are automatically detected and managed locally by the active nodes by regulating dynamically the active power injected into the grid, as described in Fig. 3.

Fig. 10 shows the voltage deviation at the point of connection of EG_2. This node is more affected by these phenomena since it is the farthest from the PCC. In particular, the figure shows how the overvoltage control feature integrated into the control scheme allows an accurate and precise limitation of voltage magnitude at critical nodes. In the considered case, the power that cannot be injected into the grid due to overvoltage limitations is stored in the local accumulators, if compatible with the corresponding state of charge, otherwise the generation is curtailed by acting on the power point tracker, as, for example, in [21], [30].

Indeed, to meet the $\Delta v_{\%}^{\max}$ constraint can necessarily lead to a reduced power production from renewables in grids where the distribution lines have high R/X ratios. Fig. 11 reports the profile of the total maximum power that can be ideally extracted from PV sources and the actual total power production obtained in *Case B* and *Case C*. Since the power injection is limited during an overvoltage condition, the power in excess is totally curtailed in *Case C*, whereas, in *Case B*, it is curtailed for only the portion that cannot be stored in the local ES. Fig. 12 shows the corresponding SOC of the ES of the two energy gateways; due to the proportional contribution from the EGs, SOC behaviors are similar.

The behavior of coefficients α_P and α_Q along the considered simulation scenario is reported in Fig. 14, just for *Case C*. In *Case B* similar behaviors are obtained for what concerns the coefficient α_Q, while the coefficient α_P assumes only the values corresponding to the operating modes *1)* and *4)* of Section IV-A, due to the absence of storage devices. In this last case, the power output from EGs are steadily equal to the maximum power that can be generated locally while complying with the overvoltage constraint $\Delta v_{\%}^{\max}$.

5) Performance indexes: In order to emphasize the main results illustrated so far, Table IV reports some performance indexes applied to the considered application example. In particular, the total produced energy, the energy dissipated in distribution lines, the overvoltage measured at grid nodes, and the power factor measured at the PCC are reported. We notice the following aspects:

- The measured distribution losses in *Case B* are reduced by $20\,\%$ with respect to *Case A*. A further reduction by $25\,\%$ can be achieved with the integration of energy storage devices at active nodes (*Case C*). The maximum

This article has been accepted for publication in a future issue of this journal, but has not been fully edited. Content may change prior to final publication. Citation information: DOI 10.1109/JESTPE.2015.2413361, IEEE Journal of Emerging and Selected Topics in Power Electronics

TABLE IV
PERFORMANCE INDEXES COMPUTED AT MICROGRID PCC

	Produced Energy (kWh)	Distribution Loss (kWh)	v_{EG1} max overvoltage (%)	v_{LOAD} max overvoltage (%)	v_{EG2} max overvoltage (%)	PCC Power Factor
Case A – No Control	36.5	0.83	1.4	2.4	5.5	0.93
Case B – PB Control	34.1	0.65	1.2	1.8	4.0	1.00
Case C – PB Control + ES	34.2	0.47	1.2	1.8	4.0	1.00

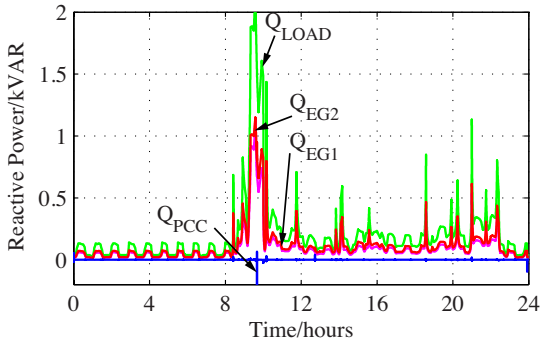

Fig. 13. Reactive power contributions from EG_1, EG_2, and the PCC, together with the absorbed load power.

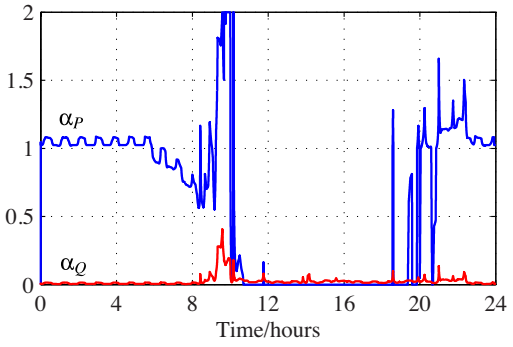

Fig. 14. Behavior of coefficients α_P and α_Q (*Case C*).

registered overvoltage stays within the programmed 4 % limit (see Table I) when the corresponding control functionality is active, i.e., in *Case B* and *Case C*. On the other hand, if no provisions are taken, *Case A* reveals a maximum reached overvoltage of 5.5 %.

- In the considered application example, the power-based control accomplishes the full compensation of the reactive power produced by the loads, achieving a unity power factor measured at the PCC. Fig. 13 shows the obtained share of reactive power between EG_1, EG_2, and the PCC, together with the reactive power absorbed by the load.
- Thanks to the effective management of the generated and stored energy performed by the proposed control scheme, a reduction of only 6 % in the total produced energy can be noticed in spite of the stringent overvoltage limitation of 4 % with respect to the nominal value V_{GRID}.

B. Experimental Results

A laboratory scale microgrid prototype has been developed to replicate the case study shown in Fig. 4. In the considered implementation, the MC resides in the UI and broadcasts once every 0.25 s the power commands to EGs, as described in Section IV. The two EGs have the same power rating of 3 kVA, and a local power availability such that $\left(\hat{P}_{G1}^{\min}, \hat{P}_{G1}, \hat{P}_{G1}^{\max}\right) = (0, 0, 0.8)$ kW and $\left(\hat{P}_{G2}^{\min}, \hat{P}_{G2}, \hat{P}_{G2}^{\max}\right) = (0, 0, 3.0)$ kW. Circuit breakers CB_1 and CB_2 connect the microgrid to the mains. CB_1 is driven by an external agent (e.g., the DSO), whereas CB_2 is an electromechanical device driven by the UI.

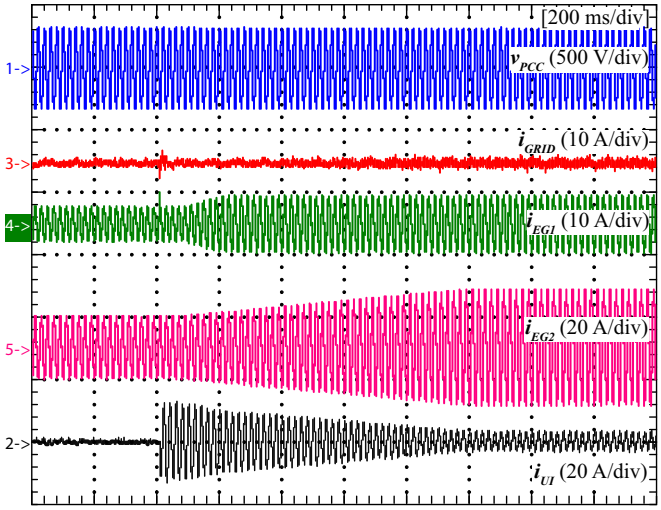

Fig. 15. Load step (2 kW to 4 kW) during grid-connected operation.

Fig. 15 shows the system response to a load step from 2 kW to 4 kW during the grid-connected operation. Initially the grid power reference P_{GRID}^{*} is equal to zero and the power absorbed by the load is 2 kW. In this situation the two EGs can completely supply the load needs and the coefficient α_P is equal to 1.526. Immediately after the step transition the UI promptly supply the load needs, while the power-based control gradually adjusts the power contribution from the EGs. Since the load absorption after the transient, equal to 4 kW, exceeds the total power availability of EGs, equal to 3.8 kW, the coefficient α_P in steady-state is equal to 2. This corresponds to the operating mode *4)* of Section IV-A, where the EGs deliver the maximum locally available power, while the UI delivers the power needed to ensure the power balance.

For a comparison with other approaches, we remark that the dynamic response of the PB control in the experimental setup is determined by the control cycle duration, the response speed of the local current controller, and the communication bandwidth. The dynamics shown in Fig. 15 are dominated by

This article has been accepted for publication in a future issue of this journal, but has not been fully edited. Content may change prior to final publication. Citation information: DOI 10.1109/JESTPE.2015.2413361, IEEE Journal of Emerging and Selected Topics in Power Electronics

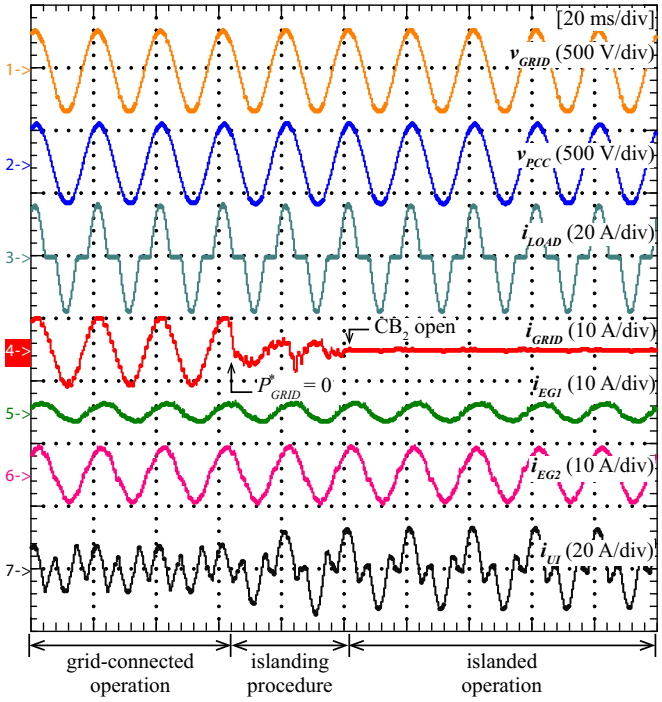

Fig. 16. Intentional transition to islanded operation.

the current controller of EG_2, that presents a constraint on the maximum rate of change of the injected current, to limit the stress to its hardware. We observe that, by removing this constraint, the response speed would be limited by only the power measurement calculations and the communication bandwidth. Neglecting the effect of the communication bandwidth, in the considered scenario the power measurement calculation bandwidth represents the upper bound for both the response speed of the power sharing among EGs and the achievable bandwidth of the power flow regulation at the PCC. The same upper bound is present in conventional droop-control schemes, for what concerns the primary control (defining the power sharing among DERs), while the tertiary control layer (concerning the regulation of the power flow at the PCC), intrinsically, has even slower response times [15], [34].

The behavior of the microgrid in response to an intentional islanding, due to, e.g., a pre-scheduled maintenance, is shown in Fig. 16. During the event a non-linear load absorbing 2 kW with crest factor $CF = 1.8$ is connected. Initially, the system operates grid-connected; the load is supplied by the two EGs ($P_{G1} = 0.25\,\text{kW}$, $P_{G2} = 0.85\,\text{kW}$) and the grid ($P_{GRID} = 0.9\,\text{kW}$), while the UI performs the harmonic compensation, guaranteeing a clean grid current ($\text{THD}_{i_g} = 4.2\,\%$), despite the heavily distorted load current ($\text{THD}_{i_{LOAD}} = 48\,\%$). The transition to the islanded operation is managed by the MC, that sets the grid power reference P^*_{GRID} to zero and then opens CB_2. The UI keeps maintaining its output voltage, and becomes the grid-forming source for the entire microgrid. Instantaneous power balance and grid voltage continuity are thus ensured by construction, together with a seamless transition from grid-connected to islanded operation.

VII. Conclusion

A simple approach to the synergistic control of distributed energy resources in low-voltage microgrids was presented and analyzed. It only requires non-time-critical power data to be transferred from the active nodes to a centralized controller through a narrowband communication link. The centralized controller, in turn, broadcasts active and reactive power set-points for all the active nodes.

Thanks to a Utility Interface converter located at the PCC, the proposed control is capable of driving the microgrid in both grid-connected and islanded operation, even during fast transients, while guaranteeing a proper power sharing between distributed resources, a regulated power flow at the PCC, and preventing the overload of DER converters.

The controller was tested by simulations and a basic application example has been presented and discussed. The results have shown that the centralized power-based control strategy smoothes the active power exchanged at PCC, significantly reduces the power losses, and avoids local overvoltages.

Finally, the experimental verification of the short-term energy flow control capability has been presented, which demonstrates the good control performance, in line with theoretical expectations.

References

[1] M. Shahidehpour, S. Pullins *et al.*, "The maturation of Microgrids," *Electrification Magazine*, vol. 2, no. 1, 2014.
[2] U.S. Energy Information Administration, "Independent Statistics and Analisis," 2013. [Online]. Available: www.eia.gov/electricity
[3] N. Hatziargyriou, *Microgrids: Architectures and Control*. Wiley-IEEE Press, 2014.
[4] B. M. Eid, N. A. Rahim, J. Selvaraj, and A. H. El Khateb, "Control Methods and Objectives for Electronically Coupled Distributed Energy Resources in Microgrids: A Review," *IEEE Systems Journal*, pp. 1–13, 2014.
[5] J. M. Guerrero, J. C. Vasquez, J. Matas, L. G. de Vicuna, and M. Castilla, "Hierarchical Control of Droop-Controlled AC and DC Microgrids - A General Approach Toward Standardization," *IEEE Transactions on Industrial Electronics*, vol. 58, no. 1, pp. 158–172, Jan 2011.
[6] W. Du, Q. Jiang, M. J. Erickson, and R. H. Lasseter, "Voltage-Source Control of PV Inverter in a CERTS Microgrid," *IEEE Transactions on Power Delivery*, pp. 1–1, Aug 2014.
[7] T. Erseghe, "Distributed Optimal Power Flow Using ADMM," *IEEE Transactions on Power Systems*, vol. 29, no. 5, pp. 2370–2380, Sept 2014.
[8] S. Bolognani, R. Carli, G. Cavraro, and S. Zampieri, "Distributed reactive power feedback control for voltage regulation and loss minimization," *IEEE Transactions on Automatic Control*, vol. PP, no. 99, pp. 1–1, 2014.
[9] W. Saad, Z. Han, and H. Poor, "Coalitional Game Theory for Cooperative Micro-Grid Distribution Networks," in *IEEE International Conference on Communications Workshops (ICC'11)*, June 2011, pp. 1–5.
[10] N. Ekneligoda and W. Weaver, "Game-Theoretic Communication Structures in Microgrids," *IEEE Transactions on Power Delivery*, vol. 27, no. 4, pp. 2334–2341, Oct 2012.
[11] N. Ekneligoda and W. Weaver, "Optimal transient control of microgrids using a game theoretic approach," in *IEEE Energy Conversion Congress and Exposition (ECCE'11)*, Sept 2011, pp. 935–942.
[12] "Reference technical rules for the connection of active and passive users to the LV electrical Utilities," *CEI 0-21*, pp. 1–146, 2012.
[13] "IEEE Standard for Interconnecting Distributed Resources with Electric Power Systems," *IEEE Std 1547-2003*, pp. 1–28, 2003.
[14] T. Caldognetto and P. Tenti, "Microgrids Operation Based on Master-Slave Cooperative Control," *IEEE Journal of Emerging and Selected Topics in Power Electronics*, vol. 2, no. 4, pp. 1081–1088, Dec 2014.

This article has been accepted for publication in a future issue of this journal, but has not been fully edited. Content may change prior to final publication. Citation information: DOI 10.1109/JESTPE.2015.2413361, IEEE Journal of Emerging and Selected Topics in Power Electronics

[15] J. M. Guerrero, M. Chandorkar, T.-L. Lee, and P. C. Loh, "Advanced Control Architectures for Intelligent Microgrids - Part I: Decentralized and Hierarchical Control," *IEEE Transactions on Industrial Electronics*, vol. 60, no. 4, pp. 1254–1262, April 2013.

[16] E. Planas, A. Gil-de Muro, J. Andreu, I. Kortabarria, and I. Martínez de Alegría, "General aspects, hierarchical controls and droop methods in microgrids: A review," *Renewable and Sustainable Energy Reviews*, vol. 17, pp. 147–159, Jan 2013.

[17] S. Bolognani and S. Zampieri, "A Distributed Control Strategy for Reactive Power Compensation in Smart Microgrids," *IEEE Transactions on Automatic Control*, vol. 58, no. 11, pp. 2818–2833, Nov 2013.

[18] P. Tenti, A. Costabeber, T. Caldognetto, and P. Mattavelli, "Cooperative control of smart micro-grids based on conservative power commands," *11th Conference-Seminar International School on Nonsinusoidal Currents and Compensation (ISNCC'13)*, vol. 89, no. 6, pp. 32–40, 2013.

[19] A. Hooshmand, H. A. Malki, and J. Mohammadpour, "Power flow management of microgrid networks using model predictive control," *Computers & Mathematics with Applications*, vol. 64, no. 5, pp. 869–876, 2012.

[20] M. Sechilariu, B. Wang, and F. Locment, "Building Integrated Photovoltaic System With Energy Storage and Smart Grid Communication," *IEEE Transactions on Industrial Electronics*, vol. 60, no. 4, pp. 1607–1618, April 2013.

[21] H. Mahmood, D. Michaelson, and J. Jiang, "A Power Management Strategy for PV/Battery Hybrid Systems in Islanded Microgrids," *IEEE Journal of Emerging and Selected Topics in Power Electronics*, vol. 2, no. 4, pp. 870–882, Dec 2014.

[22] P. Tenti, T. Caldognetto, S. Buso, and A. Costabeber, "Control of Utility Interfaces in Low-Voltage Microgrids," *5th International Symposium on Power Electronics for Distrbuted Generation (PEDG'14)*, 2014.

[23] Z. Liu and J. Liu, "Indirect Current Control Based Seamless Transfer of Three-phase Inverter in Distributed Generationase Inverter in Distributed Generation," *IEEE Transactions on Power Electronics*, vol. 29, no. 7, pp. 3368–3383, July 2014.

[24] J.-Y. Kim, S.-K. Kim, and J.-H. Jeon, "Coordinated state-of-charge control strategy for microgrid during islanded operation," in *3rd IEEE International Symposium on Power Electronics for Distributed Generation Systems (PEDG'12)*, June 2012, pp. 133–139.

[25] K. Jong-Yul, J. Jin-Hong, K. Seul-Ki, C. Changhee, P. June Ho, K. Hak-Man, and N. Kee-Young, "Cooperative Control Strategy of Energy Storage System and Microsources for Stabilizing the Microgrid during Islanded Operation," *IEEE Transactions on Power Electronics*, vol. 25, no. 12, pp. 3037–3048, Dec 2010.

[26] M. Erickson, T. Jahns, and R. Lasseter, "Comparison of PV Inverter Controller Configurations for CERTS Microgrid Applicationsof pv inverter controller configurations for certs microgrid applications," in *IEEE Energy Conversion Congress and Exposition (ECCE'11)*, Sept 2011, pp. 659–666.

[27] X. Wang, F. Blaabjerg, and W. Wu, "Modeling and Analysis of Harmonic Stability in an AC Power-Electronics-Based Power System," *IEEE Transactions on Power Electronics*, vol. 29, no. 12, pp. 6421–6432, Dec 2014.

[28] X. Wang, F. Blaabjerg, M. Liserre, Z. Chen, J. He, and Y. Li, "An Active Damper for Stabilizing Power-Electronics-Based AC Systems," *IEEE Transactions on Power Electronics*, vol. 29, no. 7, pp. 3318–3329, July 2014.

[29] Y. Yang, F. Blaabjerg, and H. Wang, "Constant power generation of photovoltaic systems considering the distributed grid capacity," in *Twenty-Ninth Annual IEEE Applied Power Electronics Conference and Exposition (APEC'14)*, March 2014, pp. 379–385.

[30] A. Ahmed, L. Ran, S. Moon, and J.-H. Park, "A Fast PV Power Tracking Control Algorithm With Reduced Power Mode," *IEEE Transactions on Energy Conversion*, vol. 28, no. 3, pp. 565–575, Sept 2013.

[31] G. Mokhtari, A. Ghosh, G. Nourbakhsh, and G. Ledwich, "Smart Robust Resources Control in LV Network to Deal With Voltage Rise Issue," *IEEE Transactions on Sustainable Energy*, vol. 4, no. 4, pp. 1043–1050, Oct 2013.

[32] T. Stetz, F. Marten, and M. Braun, "Improved Low Voltage Grid-Integration of Photovoltaic Systems in Germany," *IEEE Transactions on Sustainable Energy*, vol. 4, no. 2, pp. 534–542, April 2013.

[33] P. Tenti, A. Costabeber, F. Sichirollo, and P. Mattavelli, "Minimum loss control of low-voltage residential microgrids," in *38th Annual Conference on IEEE Industrial Electronics Society (IECON'12)*, 2012, Conference Proceedings, pp. 5650–5656.

[34] X. Lu, J. Guerrero, K. Sun, J. Vasquez, R. Teodorescu, and L. Huang, "Hierarchical control of parallel ac-dc converter interfaces for hybrid microgrids," *IEEE Transactions on Smart Grid*, vol. 5, no. 2, pp. 683–692, March 2014.

Tommaso Caldognetto (S'10) received the M.Sc. degree (with honors) in electronic engineering from the University of Padova, Padova, Italy, in 2012. He is currently working toward the Ph.D. degree in the Graduate School of Information Engineering, Department of Information Engineering, University of Padova. In 2014, he was a visiting Ph.D. student at the Institute for Automation of Complex Power Systems, University of Aachen, Aachen, Germany. His research interests include control of grid-tied converters, microgrid architectures, and real-time simulation for power electronics.

Simone Buso (M'97) received the M.Sc. degree in electronic engineering and the Ph.D. degree in industrial electronics from the University of Padova, Italy, in 1992 and 1997, respectively. He is currently an Associate Professor of electronics with the Department of Information Engineering (DEI), University of Padova. His main research interests are in the industrial and power electronics fields and are specifically related to switching converter topologies, digital control of power converters, solid-state lighting and renewable energy sources.

Paolo Tenti (M'85–SM'90–F'99) is professor of Electronics at the Department of Information Engineering of the University of Padova, Italy. His main interests are industrial and power electronics and electromagnetic compatibility. His research focuses on application of modern control methods to power electronics, EMC analysis of electronic equipment and cooperative control of distributed electronic power processors in smart grids. From 1991 to 2000 Paolo Tenti was as a member of the Executive Board of the IEEE Industry Applications Society and chaired various Society Committees. In 1997 he served as IEEE IAS President. In 2000 he chaired the IEEE World Conference on Industrial Applications of Electrical Energy in Rome. For the years 2000-2001 was appointed IEEE-IAS Distinguished Lecturer on Electromagnetic compatibility in industrial equipment. From 2002 to 2008 he served the University of Padova in the capability of Department Director and Chairman of the Board of Directors. Paolo Tenti is a Fellow of the IEEE. He is also President of CREIVen, an industrial consortium for research in industrial electronics with special emphasis on electromagnetic compatibility.

Danilo Iglesias Brandao (S'14) was born in São Gonçalo do Sapucai, Brazil in 1986. He received his B.Sc and M.Sc degrees in control and automation, and electrical engineering from Universidade Estadual Paulista, Brazil in Jul/2011 and Jan/2013, respectively. He is currently a Ph.D student from University of Campinas, Brazil. He has been a scholarship student from FAPESP since 2008 and he worked at Colorado School of Mines, USA, in 2009 and in 2013 and at University of Padova, Italy, in 2014. His main interests are power filters, power quality, photovoltaic, selective compensation, distributed generation control, cooperative compensation and microgrids.